Hindawi Publishing Corporation
International Journal of Navigation and Observation
Volume 2008, Article ID 793868, 9 pages
doi:10.1155/2008/793868

Research Article

Comparison between Galileo CBOC Candidates and BOC(1,1) in Terms of Detection Performance

Fabio Dovis,[1] Letizia Lo Presti,[1] Maurizio Fantino,[2] Paolo Mulassano,[2] and Jérémie Godet[3]

[1] *Dipartimento di Elettronica, Politecnico di Torino, Corso Duca degli Abruzzi 24, 10138 Torino, Italy*
[2] *Istituto Superiore Mario Boella, Corso Castelfidardo 30/A, 10138 Torino, Italy*
[3] *Galileo Unit, European Commission DG-Tren, 28 Rue de Mot, 1049 Brussels, Belgium*

Correspondence should be addressed to Maurizio Fantino, maurizio.fantino@ismb.it

Received 31 July 2007; Revised 30 December 2007; Accepted 25 February 2008

Recommended by Gerard Lachapelle

Many scientific activities within the navigation field have been focused on the analysis of innovative modulations for both GPS L1C and Galileo E1 OS, after the 2004 agreement between United States and European Commission on the development of GPS and Galileo. The joint effort by scientists of both parties has been focused on the multiplexed binary offset carrier (MBOC) which is defined on the basis of its spectrum, and in this sense different time waveforms can be selected as possible modulation candidates. The goal of this paper is to present the detection performance of the composite BOC implementation of an MBOC signal in terms of detection and false alarm probabilities. A comparison among the CBOC and BOC(1,1) modulations is also presented to show how the CBOC solution, designed to have excellent tracking performance and multipath rejection capabilities, does not limit the acquisition process.

1. INTRODUCTION

The agreement reached in 2004 by United States (US) and European Commission (EC) [1] focused on the Galileo and GPS coexistence clearly stated as central point to the selection of a common signal in space (SIS) baseline structure that is the BOC(1,1). In addition, the same agreement paved the way for common signal optimization with the goal to provide increased performance as well as considerable flexibility to receiver manufacturers.

Therefore, EC and US started to analyze possible innovative modulation strategies [2] in the view of Galileo E1 OS optimization and for the future L1C signals of the new generation GPS satellites.

Considering the recent activities carried out by the Galileo signal task force (STF) jointly to US experts in the Working Group A, it came out that the multiplexed binary offset carrier (MBOC) could be a good candidate for both GPS and Galileo satellites. In fact, on the 26th of July 2007 US and EC announced their decision to jointly implement the MBOC on the Galileo open service (OS) and the GPS IIIA civil signal as reported in [3].

The MBOC power spectral density (PSD) is a mixture of BOC(1,1) spectrum and BOC(6,1) spectrum; then different time waveforms can be combined to produce the MBOC-like spectral density. The contribution of the BOC(6,1) subcarrier brings in an increased amount of power on higher frequencies, which leads to signals with narrower correlation functions and then yielding better performance at the receiver level.

The European approach to the MBOC implementation consists in adding in time a BOC(1,1) and a BOC(6,1), defined as composite BOC (CBOC) modulation. At the time of writing, the US is likely to choose a time-multiplexed implementation, named TMBOC. Throughout the paper, the CBOC features will be described and clarified taking also into account different implementation options like, for example, the allocation of the power among the data and pilot channels of the E1 signal.

Regardless the kind of CBOC, such a signal structure allows the receivers to obtain high performance in terms of multipath rejection and tracking [4, 5]. This is mainly due to a higher transition rate brought by the BOC(6,1) on top of the BOC(1,1). However, the optimization process

must also consider the signal candidates in terms of their acquisition performance. It is known that CBOC signals have sharper correlation functions [4, 5] than the BOC(1,1) solution and this characteristic, as described in [6, 7], makes the acquisition process more challenging. In this paper, the acquisition of a CBOC signal in terms of its detection and false alarm probabilities (more related to the modulation characteristics and less connected to the acquisition implementation) is investigated and compared to the performance of the pure BOC(1,1) modulation as well as the detection performance of a BOC(1,1) legacy receiver acquiring a CBOC signal. In this paper, the mean acquisition time is not investigated, since it is connected to the detection rate performance as well as the acquisition solution being implemented, so not only dependent on the signal modulation itself.

The results show that from the acquisition standpoint, thanks to the 10/11th of power located to a BOC(1,1) in the MBOC spectrum, the compatibility with the state-of-the-art BOC(1,1) receiver baseline is assured.

Moreover, it is assumed to use the Galileo acquisition engines presented in [8] which work on a pilot channel with a secondary code, that further modulates the primary pseudorandom sequences (any kind of BOC or MBOC).

The paper is organized as follows: Section 2 reports the main features of the MBOC approach while Section 3 presents the correlations properties as well as the possible CBOC candidates in terms of power allocation. Then, Section 4 is devoted to the description of the acquisition problem from a theoretical aspect, and Section 5 presents the related simulation results for the CBOCs and BOC(1,1) modulated signals. Finally, Section 6 draws some conclusions.

2. MBOC DEFINITION AND SPECTRUM CHARACTERISTICS

As reported in [9], the MBOC signal is obtained defining its power spectral density as a combination of the BOC(1,1) and BOC(6,1) power spectra (i.e., including both pilot and data channel components). The notation introduced in [9] is MBOC(6,1,1/11), where the term (6,1) refers to the BOC(6,1), and the ratio 1/11 represents the power split between the BOC(1,1) and BOC(6,1) spectrum components as given by

$$G_{\mathrm{MBOC}}(f) = \frac{10}{11} G_{\mathrm{BOC}(1,1)}(f) + \frac{1}{11} G_{\mathrm{BOC}(6,1)}(f), \quad (1)$$

where $G_{\mathrm{BOC}(m,n)}(f)$ is the unit-power spectrum density of a sine-phased BOC modulation as defined in [10].

Figure 1 shows the comparison among the PSDs of the BOC(1,1) and the MBOC(6,1,1/11) foreseen for the Galileo E1 signal as well as for the future GPS L1C. In the picture, it is evident that the increased power at a frequency shifted about 6 MHz from the central frequency E1, deriving by the presence of the BOC(6,1) component.

It is important to remark that MBOC is defined starting from the power spectrum. In this sense, many possible time-domain implementations can result with the same approximation of the defined spectrum.

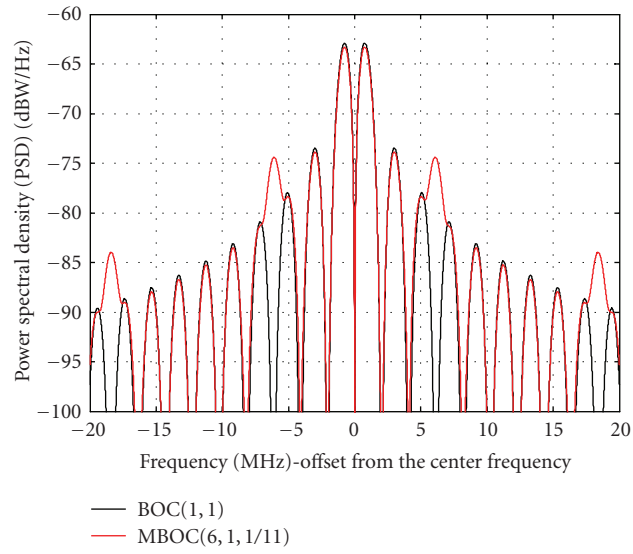

Figure 1: Unit power spectral densities comparison of BOC(1,1) and MBOC(6,1,1/11). (Equivalent baseband representation of the E1 carrier signals.)

3. CBOC FEATURES

In CBOC implementations, each ranging code is modulated by a weighted combination of a BOC(1,1) and a BOC(6,1) subcarriers:

$$s_{\mathrm{BOC}(1,1)}(t) = \begin{cases} \mathrm{sign}\left[\sin\left(\frac{2\pi t}{T_C}\right)\right], & 0 \le t \le T_C, \\ 0, & \text{elsewhere}, \end{cases}$$
$$s_{\mathrm{BOC}(6,1)}(t) = \begin{cases} \mathrm{sign}\left[\sin\left(\frac{12\pi t}{T_C}\right)\right], & 0 \le t \le T_C, \\ 0, & \text{elsewhere}, \end{cases} \quad (2)$$

where $T_C = 1/(1.023 \cdot 10^6)$ [second] is the chip duration.

The notation usually reported for the composite BOC signal is CBOC(6,1,γ/ρ), where the parameters γ and ρ are related to the power splitting between the BOC(1,1) modulated signal and the BOC(6,1) contribution. However, such a notation does not take into account that the actual overall signal is obtained by combining data and pilot channels, then introducing a further degree of freedom. Furthermore, it is not mandatory that the BOC(6,1) contribution has to be present on both data and pilot channels, opening additional options to the implementation.

Therefore, the time-domain signal on the E1 data channel can be expressed as

$$s_{\mathrm{E1}}^{tx}(t) = x_{\mathrm{E1},d}(t) \cdot \alpha \left[\sqrt{\frac{\rho - \gamma}{\rho}} s_{\mathrm{BOC}(1,1)}(t) + k_d \sqrt{\frac{\gamma}{\rho}} s_{\mathrm{BOC}(6,1)}(t) \right], \quad (3)$$

where $x_{\mathrm{E1},d}(t)$ is the product of the navigation message and the spreading code, and α is the fraction of power allocated

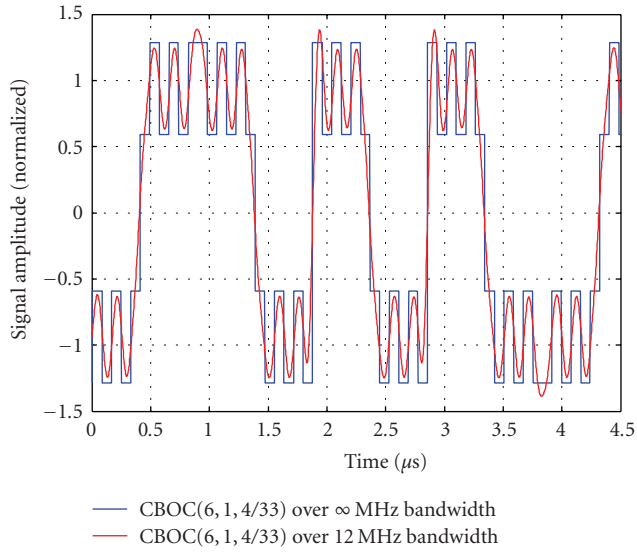

Figure 2: Example of a CBOC(6,1,1/11) over an infinite bandwidth (blue line) and shaped with a 12 MHz, 4 pole, Butterworth filter (red line).

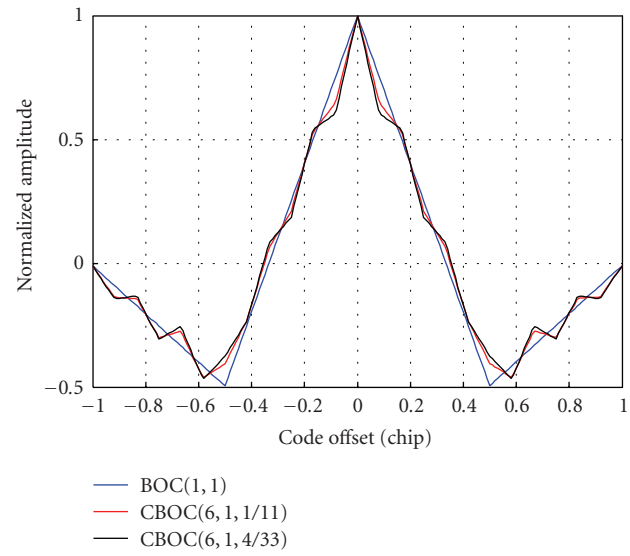

Figure 3: Normalized autocorrelation functions comparison of BOC(1,1), CBOC(6,1,1/11), and CBOC(6,1,4/33) computed over an infinite bandwidth.

Table 1: Possible options for the MBOC signal implementation by means of CBOC modulations.

Data channel modulation	Data channel power	Pilot channel modulation	Pilot channel power
CBOC(6,1,1/11)	25%	CBOC(6,1,1/11)	75%
CBOC(6,1,1/11)	50%	CBOC(6,1,1/11)	50%
BOC(1,1)	25%	CBOC(6,1,4/33)	75%

to the data channel. In the same way, the E1 pilot channel can be expressed as

$$s_{\mathrm{E1}}^{tx}(t) = x_{\mathrm{E1},p}(t)\cdot\beta\left[\sqrt{\frac{\rho-\gamma}{\rho}}s_{\mathrm{BOC}(1,1)}(t)+k_p\sqrt{\frac{\gamma}{\rho}}s_{\mathrm{BOC}(6,1)}(t)\right], \tag{4}$$

where $x_{\mathrm{E1},p}(t)$ is the spreading code sequence, and β is the fraction of power allocated to the pilot channel.

The parameters k_d and k_p can assume the values $(0, \pm 1)$, and they are used to model the presence or not of the BOC(6,1) subcarrier and its sign in the channels.

It is important to remark that, under the assumption that data and pilot channels use orthogonal spreading codes, the residual cross-correlation between the spreading sequences chosen for Galileo can be considered negligible, the overall spectrum on the E1 band is the summation of the power spectra of the pilot and data channels. Different combinations of the parameters α, β, k_d, k_p, γ, and ρ can be chosen in order to obtain signals, whose power spectral density resembles the spectral mask defined for the MBOC signal.

Table 1 shows some possible selection of the parameters associated to the power split between data and pilot channels.

As already remarked, it is not always the case that the CBOC is selected for both data and pilot channels (see third row of Table 1). Anyway, the most probable implementation selected by EC will fall on the CBOC(6,1,1/11) option (and both k_d and k_p positive) with 50% of power on both channels. This decision is due to the relatively high data rate on the E1 data channel, which is known also to carry integrity messages.

Regardless the power splitting, the CBOC in time-domain shows a four-level spreading sequence as depicted in Figure 2, where a CBOC(6,1,1/11) realization with positive contribution coming from the BOC(6,1) subcarrier has been reported.

The presence of higher transition rate (due to BOC(6,1) component) creates a sharper correlation function than the BOC(1,1) baseline. The normalized autocorrelation functions of the CBOC(6,1,1/11) and CBOC(6,1,4/33) are compared to the BOC(1,1) correlation in Figure 3.

The larger is the contribution of the BOC(6,1) subcarrier (as so the γ over ρ ratio) in the CBOC implementation, the sharper is the correlation function.

This characteristic will be deeply highlighted in the following sections considering its impact on the detection performance of the acquisition stage of the receiver.

To better highlight the sharper CBOC correlation functions, a zoom of Figure 3 around the main peak is reported in Figure 4.

The CBOC autocorrelation function can be written by means of the BOC(1,1) and BOC(6,1) autocorrelations and cross-correlations as

$$\begin{aligned} R_{\mathrm{CBOC}(6,1,\gamma/\rho)}(\tau) = {} & \frac{\rho-\gamma}{\rho}R_{\mathrm{BOC}(1,1)}(\tau) \\ & + \frac{\gamma}{\rho}R_{\mathrm{BOC}(6,1)}(\tau) \\ & + 2\frac{\gamma}{\rho}\sqrt{\frac{\rho}{\gamma}-1}\,R_{\mathrm{BOC}(1,1)\mathrm{BOC}(6,1)}(\tau), \end{aligned} \tag{5}$$

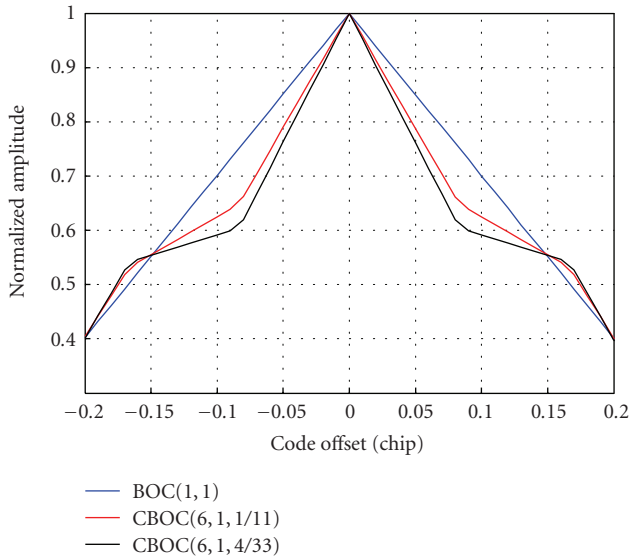

Figure 4: Zoom of the normalized autocorrelation functions comparison among BOC(1,1), CBOC(6,1,1/11), and CBOC(6,1,4/33) computed over an infinite bandwidth.

where the term $R_{\mathrm{BOC}(1,1)\mathrm{BOC}(6,1)}(\tau)$ is the cross-correlation term between the BOC(1,1) and BOC(6,1).

The presence of a cross-correlation factor in (5) results in creating little differences with respect to the MBOC spectrum as defined in (1). Therefore, on-going studies are in place with the goal to define implementation strategies to remove such cross factor. Among the others, the most promising is to alternate BOC(6,1) and BOC(1,1) phases on adjacent code chips (see as an example [11]).

4. ACQUISITION OF THE OPTIMIZED CBOC SIGNAL

The first operation performed by any GNSS receiver is the signal acquisition, in charge to understand which satellites are in the line of sight and to provide the tracking stages with a coarse estimation of the received code delay and a rough estimation of the Doppler frequency shift.

The declaration of the presence or absence of a satellite (determination of both code delay and Doppler shift) is obtained by evaluating a two-dimensional matrix called search space. Each item of such a matrix, that is, cell, corresponds to the value assumed by the bi-dimensional correlation for a specific couple code delay $\hat{\tau}$ and Doppler shift $\hat{f}_d$. This bi-dimensional correlation is also known as cross-ambiguity function.

As shown in [8], several are the solutions that can be found in literature for the signal acquisition: serial search, fast acquisition, and parallel acquisition in frequency domain, but they just differ in the way the search space is obtained and equivalent in terms of detection performance. Other acquisition techniques known with the name of differential acquisition strategies are nowadays used in GNSS fields [12], but since the mathematical details are different from the previous mentioned methodologies, they will not be considered in this paper.

Any acquisition technique can be characterized for a given C/N_0 by the false alarm and detection probabilities. Here, just the false alarm and detection cell probabilities will be considered, since as discussed in [13] the characteristics of the acquisition engine can always be related to these fundamental values.

Such probability functions are usually evaluated considering only the peak amplitude of the correlation function and the presence of noise. Such characterization does not take into account the fact that, for a given Doppler shift and code phase error, the correlation generally does not achieve the maximum possible value. This effect can be modeled as a correlation loss which depends on the shape of the cross ambiguity function and on its representation in terms of resolution (i.e., Doppler shift and code delay steps) in the search space [8].

In order to take into account also this effect in the comparison of BOC(1,1) and CBOC(6,1,γ/ρ) functions, the behavior around the peak in the search space has to be studied.

Once decided the acquisition threshold V_t, the cell false alarm probability can be easily evaluated as the integral of the tail of the distribution of the search matrix in a misalignment condition (or equivalently when the signal is absent). In formula is (see [14])

$$P_{fa}(V_t) = \int_{V_t}^{+\infty} f_{na}^{K}(x)dx. \tag{6}$$

The distribution of $f_{na}^{K}(r)$ can be shown to assume the expression [8]:

$$f_{na}^{K}(r) = \frac{1}{2^K(K-1)!\sigma^{2K}} r^{K-1} e^{-r/2\sigma^2} u(r), \tag{7}$$

where, when the local code spreading sequence has unitary power, and the signal is digitized respecting the Nyquist criterion, σ^2 is equal to $(N/2)\sigma_n^2$. N is the number of samples coherently integrated, and σ_n^2 is the variance of the Gaussian noise affecting the received signal.

Equation (7) holds for the case of noncoherent integration process applied to a serial or parallel acquisition technique. With this technique, the detection and decision can be taken over the summation of K correlation outputs before the envelope operation so to reduce the noise impact and to increase the acquisition detection rate [8].

The probability density function of the correlator output depends on two variables: the code displacement error $\Delta\tau = \tau - \hat{\tau}$ and the Doppler shift error $\Delta f_d = f_d - \hat{f}_d$, respectively. The conditional probability density function to the hypothesis of a perfect code and Doppler alignment $(\Delta\tau = 0, \Delta\tau = 0)$ is demonstrated in [8] to assume the expression:

$$f_a^K(r \mid \Delta\tau, \Delta f_d = 0) = \frac{\sqrt{K}\alpha}{\sigma^2}\left(\frac{r}{\sqrt{K}\alpha}\right)^K e^{-(1/2)((r^2+K\alpha^2)/\sigma^2)} I_{K-1}\left(r\frac{\sqrt{K}\alpha}{\sigma^2}\right), \tag{8}$$

where $\alpha = \sqrt{C}N/2$ is a term proportional to the received signal power C. The corresponding conditional detection probability is then the integral over the tail of $f_a^K(r \mid \Delta\tau, \Delta f_d = 0)$ (see [8, 15]), which leads to the expression:

$$P_{d|\Delta\tau,\Delta f_d=0}(V_t) = \int_{\sqrt{V_t}/\sigma}^{+\infty} f_a^K(x)dx = Q_K\left(\frac{\alpha}{\sigma}, \frac{\sqrt{V_t}}{\sigma}\right). \quad (9)$$

Equation (9) involves the kth-order Marcum Q function, Q_K discussed and defined in [15]. It is remarked how (9) does not still consider the shape of the correlation function of the signal being acquired.

This correlation function can be locally approximated around the peak as the product of the mono-dimensional correlations along the code delay and Doppler axes [7, 8], that is

$$R(\tau, \hat{\tau}, f_d, \hat{f}_d) \approx R_{\text{Doppler}}(f_d - \hat{f}_d) R_{\text{Code}}(\tau - \hat{\tau}). \quad (10)$$

It is evident that in real applications, where a residual error remains in the estimation of the code phase and Doppler shift, the acquisition does not work using the maximum possible correlation value. This situation can be modeled as additional losses or as an impairment, which depends both on the shape of $R_{\text{Code}}(\Delta\tau)$ and $R_{\text{Doppler}}(\Delta f)$.

The approximation reported in (10) is extremely important because it makes possible to separate the effects of the code errors to the one coming from Doppler shift, so to consider the total loss simply as the product of two single impairments.

As far as the code error loss is concerned, the reduction of the correlation output can be accounted in a dB amplitude scale as [8]

$$\alpha_{\text{loss}}\big|_{\text{dB}} = 20\log\left|R_{\text{Code}}(\Delta\tau)\right|. \quad (11)$$

A plot of the code correlation losses for the CBOC(6,1,1/11), CBOC(6,1,4/33), and the BOC(1,1) is depicted in Figure 5.

Similarly to the code correlation loss, the residual Doppler phase error in the acquisition process produces a reduction of the correlation peak that is demonstrated, again in [8], to be equal to

$$\begin{aligned}\beta_{\text{loss}}\big|_{\text{dB}} &= 20\log_{10}\left|R_{\text{Doppler}}(\Delta f)\right| \\ &\cong 20\log_{10}\left|D_N[\pi(f_d - \hat{f}_d)]\right|.\end{aligned} \quad (12)$$

Being $D_N(x/2) = \sin(xN/2)/N\sin(x/2)$, the Dirichlet kernel function. Remembering that the term N is the number of samples coherently integrated, it is clear how the correlation loss β_{loss} depends on the integration time. Figure 6 reports the trend of the Doppler loss when the integration time goes from $T = 4$ milliseconds up to $T = 12$ millisecondss with 4 milliseconds of step.

It is necessary to model the probability distribution of the code phase offset and Doppler shift in order to add up the different losses inside the conditional detection probability reported in (9). These two realistic hypotheses can be made

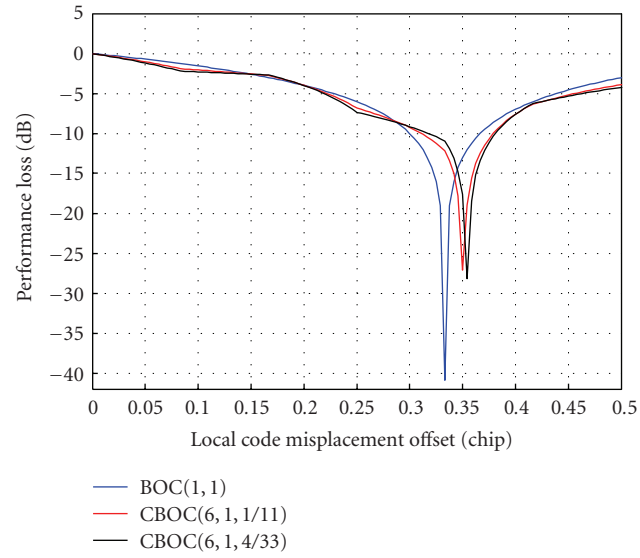

Figure 5: Performance loss as a function of the code offset for the BOC(1,1), CBOC(6,1,1/11), and CBOC(6,1,4/33).

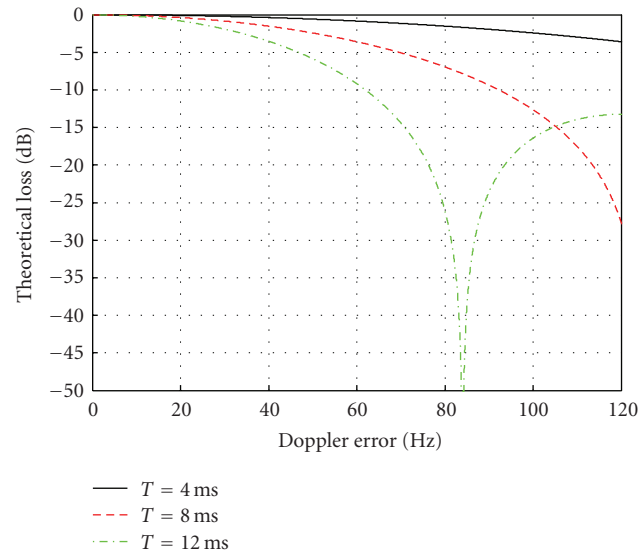

Figure 6: Logarithmic Doppler loss.

on the basis of the functioning of the acquisition engine:

(i) the resolution used in the acquisition phase is usually of some integer fraction $\pm 1/L$ of chip, then the maximum absolute phase offset $\Delta\tau = \tau - \hat{\tau}$ can be assumed uniformly distributed between $\pm 1/(2L)$ chip;

(ii) similarly, the Doppler frequency $\Delta f_d = f_d - \hat{f}_d$ can be assumed to be uniformly distributed between zero and half the maximum absolute digital frequency, obtained by normalizing a natural frequency expressed in Hz with respect to the numerical frequency used to express a sequence of sample of a digital signal, bin width $\pm 1/(2M)$, where M is typically less or equal to N.

Furthermore, the Doppler frequency and code phase errors can be considered independent and uncorrelated. With all these assumptions, the combined loss simply becomes the sum (because expressed in dB) of the contributions α_{loss} and β_{loss}. Thus, according to the definition of [6, 8], an expected value of the detection probability, which also accounts for the particular shape of the cross ambiguity function and the impairments due to the residual code phase and Doppler errors, can be derived from the conditional detection probability defined in (9) integrating over the two assumed distribution for $\Delta\tau$ and Δf_d:

$$P_d = 2N \int_{-1/2L}^{1/2L} \int_{-1/2M}^{1/2M} Q_k\left(\frac{\sqrt{k}\alpha}{\sigma} R(f,\theta), \frac{\sqrt{V_t}}{\sigma}\right) df\, d\theta, \quad (13)$$

with $R(f,\theta) = D_N(\pi f) R_{\text{Code}}(\theta)$.

Therefore, since different modulations have different $R_{\text{Code}}(\theta)$, clearly different detection rate must be expected considering what derived in (13).

The expected value of the detection rate P_d averages among all the possible code phase and Doppler offset; the acquisition can deal with, and it can be seen as an averaged probability even though in the following it will be referred to this quantity as a normal probability.

5. DETECTION PERFORMANCE OF THE CBOC MODULATION CANDIDATES

The CBOC candidates and BOC(1,1) modulations have been compared considering the impairments addressed in Section 4. Both false alarm and detection probabilities have been obtained by means of Monte Carlo simulations.

A classical acquisition technique not tailored for the new modulation has been considered, and the false alarm probability as well as the detection rate has been determined considering an integration period of 4 milliseconds (one Galileo primary code duration). All the simulated signals (BOC(1,1) and CBOCs) have been sampled at 12 MSamples/s considering the front end operating under the Nyquist criterion (i.e., 12 MHz two- sided bandwidth).

A common way to express the detection performance of an acquisition engine is by means of the so-called receiver operative characteristics (ROC) curves, where the detection probability is reported versus the false alarm probability at a specific signal to noise ratio. During this performance analysis, a C/N_0 of 40 dB·Hz has been considered to obtain all the ROC curves, where C/N_0 here refers to the single channel (pilot or data component) carrier to noise ratio.

In Figure 7, a comparison among the BOC(1,1) modulation and two different CBOC implementations is depicted. The ROC curves for the three modulations are reported changing by simulation to simulation and by the code search resolution starting from a value of half a chip down to an eighth of chip.

It is evident from this comparison that when the code search step is reduced, higher detection rates can be achieved for the same false alarm probabilities with all the modulations. These trends can be explained remembering that the larger is the code phase error $\Delta\tau$, the larger is the correlation loss averaged in (13), and then the lower is the detection rate.

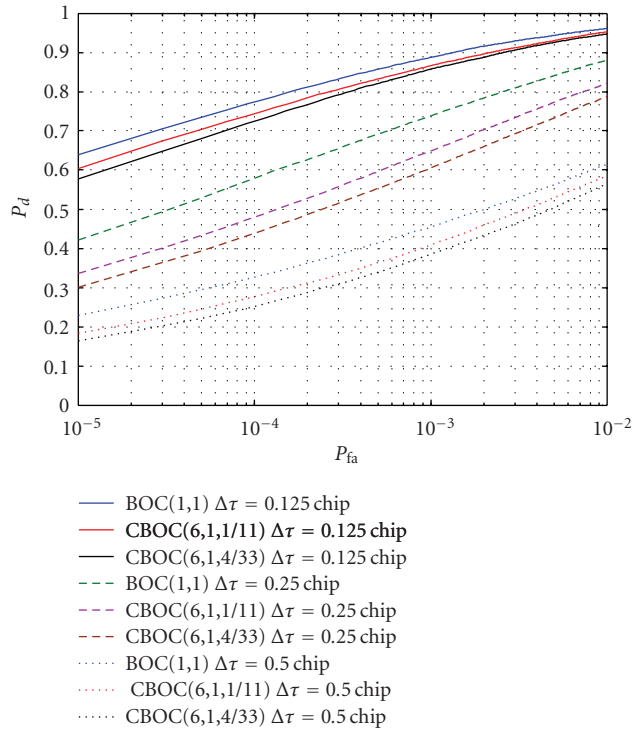

Figure 7: Receiver operative characteristic comparison among different CBOC implementations and BOC(1,1) for different search space spacing at C/N_0 of 40 dB·Hz.

The sharper correlation functions of the CBOC implementations lead to a more relevant code loss contribution with respect to the BOC(1,1). However, as demonstrated in Figure 7, the degradation which stems from the different code loss among BOC(1,1) and CBOCs can be reduced decreasing the code phase step, anyway often necessary to guarantee the pull-in phase of the tracking stages.

Another possibility to address the detection acquisition performance is given by graphs which depict the detection probability for a given false alarm probability versus the C/N_0, as done in the comparison of Figure 8.

Here, the BOC(1,1) and CBOCs modulations are compared considering a fixed false alarm probability of 10^{-4} varying the C/N_0 from a minimum of 30 up to 55 dB·Hz.

In this operative scenario, the C/N_0 necessary to acquire the CBOCs with a detection probability of 0.9 is reported in Table 2 as well as the degradation with respect to the case of using a BOC(1,1) modulation.

Considering that since MBOC has better self spectral separation coefficients (SSCs) than BOC(1,1), the intrasystem interference coming from satellites transmitting MBOC with a different PRN will be reduced.

In addition, the SSC between the MBOC and the C/A code is also lower and thus in summary the intersystem and intrasystem interference is also reduced [16]. Then, the equivalent noise due to interference from other satellites is around 0.1–0.2 dB lower for MBOC than for BOC(1,1), and

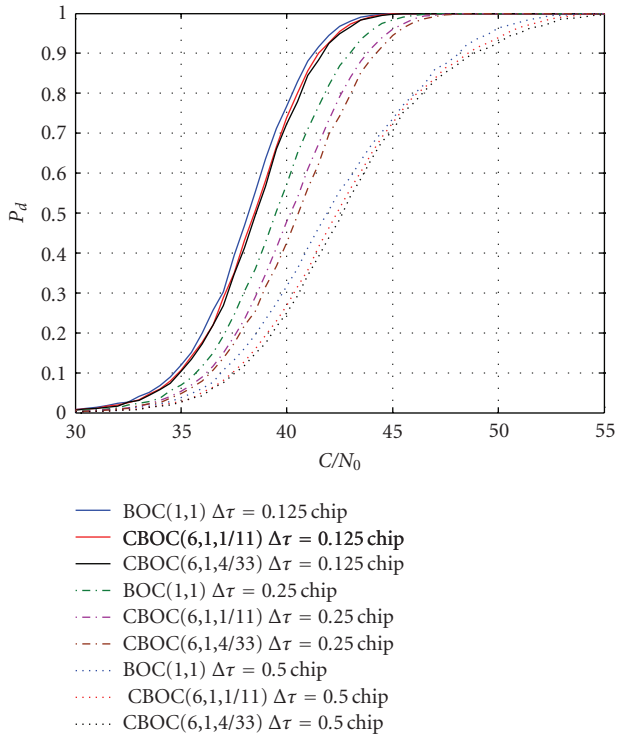

Figure 8: Detection probability versus the C/N_0 at a false alarm probability of 10^{-4}. Comparison among different CBOC implementation for different search space resolution.

Table 2: Carrier to noise ratio degradation. Comparison for CBOCs and BOC(1,1) modulations.

Modulation	Resolution [chip]	C/No @ Pd = 0.9 [dB-Hz]	Degradation w.r.t BOC(1,1) [dB-Hz]
BOC(1,1)	0.125	41.25	—
CBOC(6,1,1/11)	0.125	41.50	0.25
CBOC(6,1,4/33)	0.125	41.69	0.44
BOC(1,1)	0.25	42.95	—
CBOC(6,1,1/11)	0.25	43.78	0.83
CBOC(6,1,4/33)	0.25	44.21	1.26
BOC(1,1)	0.5	48.10	—
CBOC(6,1,1/11)	0.5	48.55	0.45
CBOC(6,1,4/33)	0.5	48.80	0.7

the equivalent C/N_0 is expected to be 0.1–0.2 dB-Hz better [16].

In addition, the interplex modulation product with MBOC is around 4 dB lower with CBOC than with BOC(1,1) and thus the net effect is that at the end, for the same transmitted power from the satellite, at the ground there is an increase of the received power of approximately another half a dB.

Therefore, the degradation of the sharper correlation function is mostly compensated in all the cases by the increased power at the ground and by better SSC, and in some cases it should actually outperform the BOC(1,1) at least when code search step is reduced to less or equal to one quarter of chip.

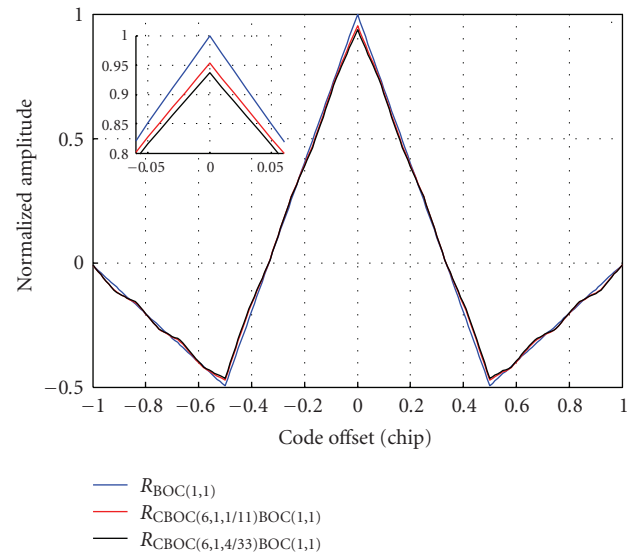

Figure 9: BOC(1,1) and CBOC cross-correlation functions comparison computed over an infinite bandwidth and zoom of correlation peaks.

It has not to be forgotten that one of the aim of the CBOC modulations is to maintain the interoperability and the compatibility with the existing systems. In fact, the contribution of the BOC(1,1) in the CBOC definition, (cfr. (3) and (4)), still assures a nonzero cross-correlation function among CBOCs and BOC(1,1).

Figure 9 reports the correlation functions obtained demodulating a CBOC signal with a local BOC(1,1) code.

This might be the working scenario of a BOC(1,1) legacy receiver processing the new optimized MBOC signal.

The cross-correlation functions $R_{CBOC(6,1,1/11)BOC(1,1)}$ and $R_{CBOC(6,1,4/33)BOC(1,1)}$ depicted in Figure 9 are practically identical.

They are mainly characterized by a reduction of the peak maximum due to the cross loss given by the BOC(6,1) term, but the correlation slope and widths are comparable one to the other.

This is the case of the ROC curves reported in Figure 10 where the detection performance of the CBOC(6,1,1/11) demodulated by a BOC(1,1) replica is reported together with the performance of the standalone BOC(1,1) and CBOC(6,1,1/11).

The comparison is made considering only a code delay step of 0.25 and 0.125 chip. The detection probability versus the C/N_0 for a false alarm probability of 10^{-4} is reported in Figure 11.

It is interesting to notice how, when the search space has a resolution of 0.25 chip for the code phase, higher detection probabilities can be obtained by demodulating the CBOC(6,1,1/11) with a local BOC(1,1) implementation. When the code step used in the search space is

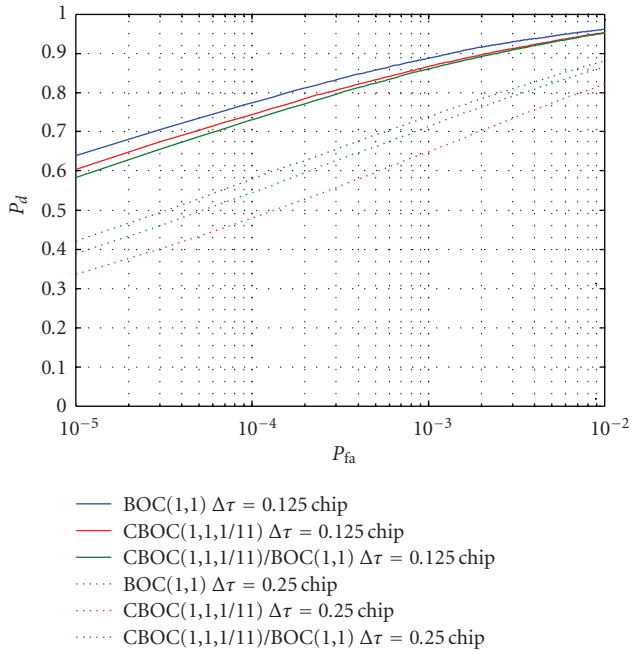

Figure 10: Receiver operative characteristic comparison, at C/N_0 of 40 dB·Hz and different spacing, among the standalone BOC(1,1), CBOC(6,1,1/11), and the CBOC(6,1,1/11) demodulated with a BOC(1,1) replica.

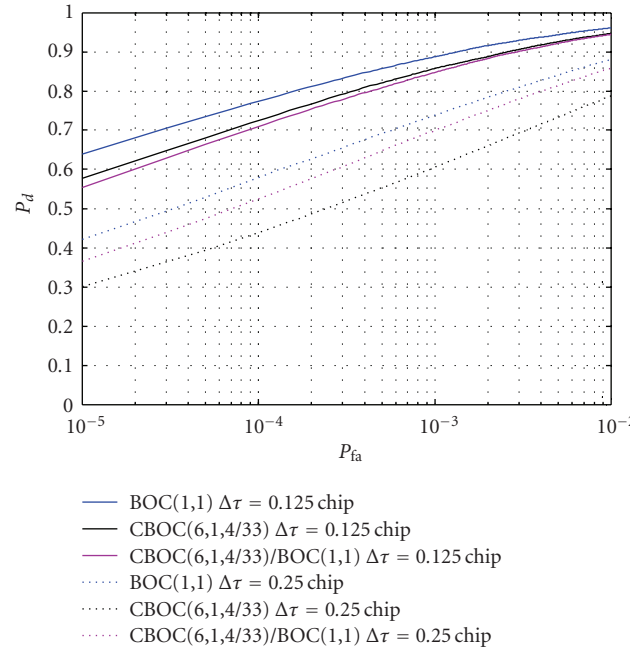

Figure 12: Receiver operative characteristic comparison, at C/N_0 of 40 dB·Hz and different spacing, among the standalone BOC(1,1), CBOC(6,1,4/33), and the CBOC(6,1,4/33) demodulated with a BOC(1,1) replica.

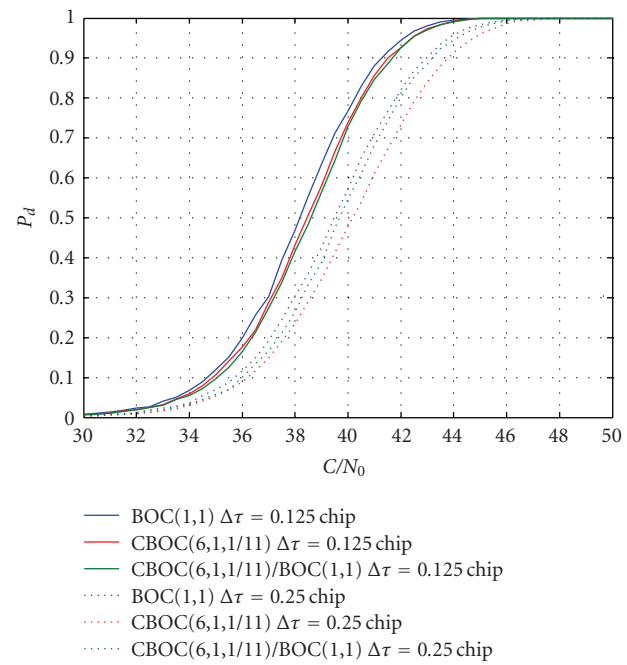

Figure 11: Detection probability versus the C/N_0 at a false alarm probability of 10^{-4} comparison among standalone BOC(1,1), CBOC(6,1,1/11), and the CBOC(6,1,1/11) demodulated with a BOC(1,1) replica.

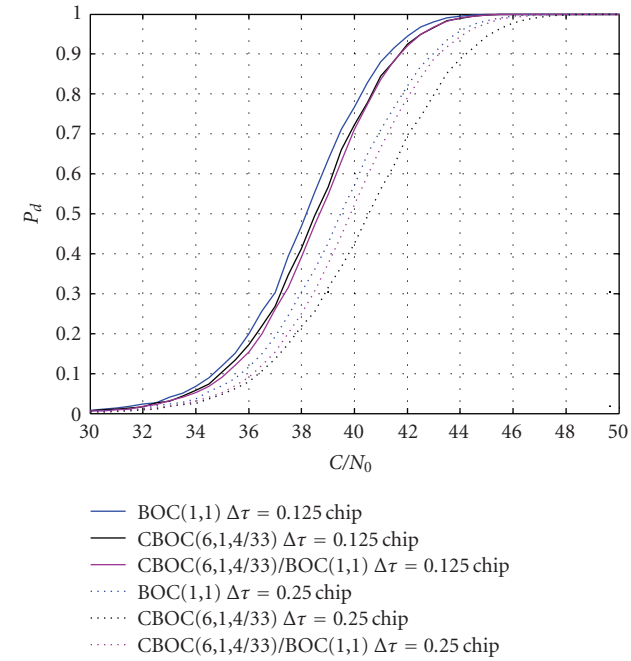

Figure 13: Detection probability versus the C/N_0 at a false alarm probability of 10^{-4} comparison among standalone BOC(1,1), CBOC(6,1,4/33), and the CBOC(6,1,4/33) demodulated with a BOC(1,1) replica.

reduced to 0.125 chip, then the solution to demodulate the CBOC(6,1,1/11) with a local BOC(1,1) does not outperform the pure CBOC(6,1,1/11) solution.

Similar considerations can be made for the comparison of the CBOC(6,1,4/33) detection performance which have been reported in Figures 12 and 13.

When $\Delta\tau$ is reduced, then the maximum peak reduction of $R_{\mathrm{CBOC(6,1,1/11)BOC(1,1)}}$ and $R_{\mathrm{CBOC(6,1,4/33)BOC(1,1)}}$ plays a more significant role in the total averaged loss explaining the change of performance outlined in the previous comments.

6. CONCLUSIONS

On the basis of the modernization activities around the future Galileo E1 signals, this paper focuses on the analysis of the acquisition detection performance of two CBOC solutions, which are the CBOC(6,1,1/11) and CBOC(6,1,4/33).

Such activity, done with an acquisition engine implemented via software, is a key step for signals comparison considering that the CBOC modulation due to its sharper correlation function might present some acquisition losses with respect to the BOC(1,1). Through simulations, it has been proved that, in practical operative conditions and thanks to the better SSC derived by using an MBOC spectrum and thanks to the increased power level of the signal at the ground (which results in about 0.7 dB·Hz of improvement in the equivalent C/N_0 seen by the receivers antennas), those losses can be neglected.

Moreover, this work also shows how the CBOC candidate modulations still assure the compatibility and interoperability with BOC(1,1) legacy receivers in terms of acquisition.

All these considerations together with the major advantages in terms of better tracking performance and multipath rejections capabilities clearly justify the selections of the CBOC as implementation of the agreed MBOC.

REFERENCES

[1] United States-European Commission Agreement on the Promotion, "Provision and Use of Galileo and GPS Satellite-Based Navigation Systems and Related Application," http://pnt.gov//public/docs/2004-US-EC-agreement.pdf.

[2] "Joint Statement on Galileo and GPS Signal Optimization By the European Commission (EC) and the United States (US)," Bruxelles March 2006, http://useu.usmission.gov/Dossiers/Galileo_GPS/Mar2406_Joint_Statement.pdf.

[3] "United States and the European Union announce final design for GPS-Galileo common civil signal," http://europa.eu/rapid/pressReleasesAction.do?reference=IP/07/1180&format=HTML&aged=0&language=EN&guiLanguage=fr.

[4] G. W. Hein, J. A. Avila-Rodriguez, L. Ries, et al., "A candidate for the Galileo L1OS optimized signal," in *Proceedings of the Institute of Navigation (ION '05)*, Long Beach, Calif, USA, September 2005.

[5] G. W. Hein, J. A. Avila-Rodriguez, S. Wallner, et al., "MBOC: the new optimized spreading modulation recommended for GALILEO L1 OS and GPS L1C," in *Proceedings of the IEEE/ION Position, Location, and Navigation Symposium (PLANS '06)*, pp. 883–892, San Diego, Calif, USA, April 2006.

[6] D. Borio, M. Fantino, L. Lo Presti, and L. Camoriano, "Acquisition analysis for Galileo BOC modulated signals: theory and simulation," in *Proceedings of the European Navigation Conference (ENC '06)*, Manchester, UK, May 2006.

[7] H. Mathis, P. Flammant, and A. Thiel, "An analytic way to optimize the detector of a post-correlation FFT acquisition algorithm," in *Proceedings of the International Technical Meeting of the Satellite Division of the Institute of Navigation (ION GPS/GNSS '03)*, pp. 689–699, Portland, Ore, USA, September 2003.

[8] M. Fantino, "Study of architectures and algorithms for software Galileo receivers," Ph.D. dissertation, Electronic Department, Politecnico di Torino, Torino, Italy, May 2006.

[9] GPS-Galileo Working Group A MBOC Recommendations, "Recommendations on L1 OS/L1C Optimization," March 2006, http://www.galileoju.com/page3.cfm.

[10] J. W. Betz, "Design and performance of code tracking for the GPS M code signal," in *Proceedings of the 13th International Technical Meeting of the Satellite Division of the Institute of Navigation (ION GPS '00)*, Salt Lake City, Utah, USA, September 2000.

[11] J. A. Avila-Rodriguez, S. Wallner, G. W. Hein, et al., "CBOC—an implementation of MBOC," in *Proceedings of the 1st CNES Workshop on Galileo Signals and Signal Processing*, Tolouse, France, October 2006.

[12] S. K. Shanmugam, R. Watson, J. Nielsen, and G. Lachapelle, "Differential signal processing schemes for enhanced GPS acquisition," in *Proceedings of the 18th International Technical Meeting of the Satellite Division of the Institute of Navigation (ION GNSS '05)*, pp. 212–222, Long Beach, Calif, USA, September 2005.

[13] D. Borio, L. Camoriano, and L. Lo Presti, "Impact of the acquisition searching strategy on the detection and false alarm probabilities in a CDMA receiver," in *Proceedings of the IEEE/ION Position, Location, and Navigation Symposium (PLANS '06)*, pp. 1100–1107, San Diego, Calif, USA, April 2006.

[14] E. D. Kaplan and C. Hegarty, *Understanding GPS: Principles and Applications*, Mobile Communications Series, Artech House, Boston, Mass, USA, 2nd edition, 2006.

[15] J. I. Marcum, "A statistical theory of target detection by pulsed radar," *IEEE Transaction on Information Theory*, vol. 6, no. 2, pp. 59–267, 1947.

[16] S. Wallner, G. W. Hein, and J. A. Avila-Rodriguez, "Interference computations between several GNSS systems," in *Proceedings of the ESA Workshop on Satellite Navigation User Equipment Technologies (NAVITEC '06)*, Noordwijk, The Netherlands, December 2006.